Early age hydration of model slag cement
Interaction among C_3S, gypsum and slag with different Al_2O_3 contents

Zhang, Yu; Wan, Zhi; de Lima Junior, Luiz Miranda; Çopuroğlu, Oğuzhan

DOI
10.1016/j.cemconres.2022.106954

Publication date
2022

Document Version
Final published version

Published in
Cement and Concrete Research

Cement and Concrete Research 161 (2022) 106954

Contents lists available at ScienceDirect

Cement and Concrete Research

journal homepage: www.elsevier.com/locate/cemconres

Early age hydration of model slag cement: Interaction among C_3S, gypsum and slag with different Al_2O_3 contents

Yu Zhang *, Zhi Wan, Luiz Miranda de Lima Junior, Oğuzhan Çopuroğlu

Microlab, Faculty of Civil Engineering and Geosciences, Delft University of Technology, Delft, the Netherlands

ARTICLE INFO

Keywords:
C_3S-gypsum-slag system
Al_2O_3
Calorimetry measurement
Ettringite and calcium monosulfoaluminate
Sulfur rich species in slag
Thermodynamic modelling

ABSTRACT

A deeper insight into SO_3/Al_2O_3 ratio including the contribution of alumina in slag at early age is required to ensure a properly sulfated slag cement. In this paper, to investigate the effect of gypsum and alumina of slag, emphasis was laid on the hydration characteristics of C_3S-gypsum-slag system during the early age, of which slag was synthesized in the laboratory with varying Al_2O_3 contents from 3.69 to 18.19 wt%.

The duration of dormant period during the hydration of C_3S depended on Al_2O_3 content of slag significantly; however, the amount of silicate reaction before the onset of aluminate reaction was independent of slag chemistry and gypsum content added. The rate of aluminate reaction was controlled by the availability of reactants, SO_4^{2-} and Al^{3+} ions in particular, which were sourced from gypsum and slag, respectively. Calcium monosulfoaluminate only occurred in mixture when slag contained a high amount of Al_2O_3 (18.19 wt% in this study) at early age, and its formation proceeded continuously at the expense of ettringite. Sulfur rich species incorporated in slag started to participate into aluminate reaction after the main hydration peak of C_3S, and it played a similar role to gypsum.

1. Introduction

Ordinary Portland cement (OPC) mainly consists of calcium silicate (C_3S and C_2S), calcium aluminate (C_3A and C_4AF) and calcium sulfate (Gypsum). Much attention has been paid to the hydration of its pure components, e.g., C_3S (the major constituent), C_3A (the most reactive constituent), and usually with gypsum, in order to generate a fundamental understanding of the hydration process and performance of cement [1–6]. It is well recognized that the other two constituents, C_2S and C_4AF, contribute little at early age due to their relatively less reactive property. Moreover, gypsum or sulfate plays a key role in hydration through the reaction with C_3A, and affects the early age performance as a result [7]. Therefore, it is important to identify the optimum amount of gypsum added into the system.

Supplementary cementitious materials (SCMs) are widely used for partial cement replacement to lower the carbon dioxide footprint of concrete productions [8–11] Meanwhile, blended cements necessitate the industry and academic to have a better understanding of sulfate requirement, rather than use the same gypsum addition in OPC system. J. Cheung et al. [12] found that SCMs added into cement resulted in an undersulfated system, particularly in the presence of admixtures. Antoni et al. [13] elucidated that optimization of gypsum content in cement-calcined clay-limestone system increased one day compressive strength by >50%. On the other hand, an early depletion of sulfate and a rapid uncontrolled reaction between aluminate phase and gypsum was found in the mixture containing cement and Ca-rich aluminosilicate glass, of which high Al_2O_3 content was observed in the glass [14]. Thus, a deep insight into SO_3/Al_2O_3 ratio including the contribution of aluminate phase from SCMs is required to ensure a properly sulfated blended cement. However, results from [15] pointed out that it was the "filler effect" related to the specific surface area provided by SCMs, rather than the chemical composition, that exerted a significant effect on sulfate balance and dominated the higher sulfate requirement of cement-calcined clay-limestone system. Due to the "filler effect", a faster precipitation of C−S−H gel phase resulted in an earlier consumption of gypsum because of absorption. After sulfate depletion, sulfate was desorbed from C−S−H gel phase and available to react with aluminate phases to form ettringite.

Blast furnace slag (slag for short), whose hydration needs activation, is a by-product from the production of pig iron and presents hydraulic

* Corresponding author.
E-mail addresses: Y.Zhang-28@tudelft.nl (Y. Zhang), Z.Wan-1@tudelft.nl (Z. Wan), L.C.MirandadeLimaJunior@tudelft.nl (L.M. de Lima Junior), O.Copuroglu@tudelft.nl (O. Çopuroğlu).

https://doi.org/10.1016/j.cemconres.2022.106954
Received 4 June 2022; Received in revised form 12 August 2022; Accepted 17 August 2022
Available online 22 August 2022

property. Blending cement with slag produces analogous hydrates compared with pure cement system. Portlandite, C−S(A)−H gel phase, ettringite, AFm phases, and a hydrotalcite-like phase are identified. According to [9,16], it is well accepted that slag chemistry changes considerably with time across the world, and the increasing or decreasing of Al_2O_3 content in slag [17,18] thus upsets the hydrate assemblage in the blended cement, e.g., the distribution of aluminum in ettringite, AFm phases, and hydrotalcite-like phase. Moreover, it is still unknown whether or not this change will further affect sulfate balance in slag cement paste at early age. On the other hand, although C_3S-C_3A-gypsum system has already been employed to investigate the sulfate balance of pure cement system [6,19], and the effect of Al_2O_3 in SCMs on sulfate balance of blended cement system has also been noticed [12–15], the interaction among C_3S-(C_3A)-slag-gypsum system at early age has not been reported specifically yet.

Therefore, the present research would like to get an insight into the interaction between aluminate and sulfate phases in cement-slag system at early age. Aluminate phases in the mixture come from two parts, one is C_3A in cement clinker and the other is Al_2O_3 in slag. Sulfate phases mainly originate from gypsum added in the cement, and a small amount also sources from sulfur rich species in slag, which will transform into sulfate eventually in an alkaline environment [20–22]. Model cement-slag system containing 30 wt% C_3S + (C_3A) + gypsum and 70 wt% slag was used throughout the research to simulate CEM III/B and highlight the effect of Al_2O_3 in slag. In this paper, the authors laid emphasis on the hydration characteristics of C_3S-gypsum-slag system at early age (until 3 days) firstly. To specify the effect of Al_2O_3 and sulfur rich species in slag, one commercial slag incorporating sulfur and three synthetic slags with varying Al_2O_3 contents from 3.69 to 18.19 wt% but without sulfur were employed. In our next publication, analytically regent C_3A would be incorporated, and the agreement and disagreement with real slag cement paste would be analyzed. Apparently, the results found in this paper and following publication can provide new prospects to understand the interaction among C_3S, C_3A, slag, and gypsum in slag cement at early age. Additionally, it also contributes to understanding the role of Al_2O_3 in slag and its effect on SO_3/Al_2O_3 ratio.

2. Material and methodology

2.1. Material

One commercial slag (S) provided by Ecocem Benelux B.V., three synthetic slags (A3, A12, A18) with different Al_2O_3 contents, and quartz (QZ) acting as reference were used in the study. Their chemical compositions determined by XRF are presented in Table 1. The particle size distribution (PSD) of slags and quartz was measured by laser diffraction and is shown in Fig. 1.

The synthetic slags used in the present research were prepared by mixing commercial slag S with AR (analytical regent) CaO, MgO, SiO_2, Al_2O_3 according to different design targets. The commercial slag S and analytical reagents added to control the exact composition in each run were mixed into a homogeneous blend by combining the materials with pure ethyl alcohol, grinding the mixture in a ball milling machine at a low speed for 2 h and drying them at 100 °C for 24 h. The dried sample paste was then ground to <200 μm in a mortar for better homogeneity. Then, it was melted in an Al_2O_3 crucible at 1550 °C in the oven for 3 h (heated from room temperature to 1550 °C at a rate of 10 °C/min and maintained at 1550 °C for 3 h). The molten liquid was water quenched to obtain glassy slag, rinsed with isopropanol and dried at 100 °C for 24 h subsequently. Finally, it was crushed and ground to required particle size distribution. For synthetic slag A3, A12 and A18, the CaO/SiO_2 ratios were maintained at approximately 1 and the amounts of MgO stabilized at about 9 wt%, while Al_2O_3 contents increased from 3.69 (A3) to 18.19 wt% (A18). In other words, the Al_2O_3 content increased with the decreasing of CaO and SiO_2 contents simultaneously.

Analytically regent C_3S and gypsum ($CaSO_4{\cdot}2H_2O$) were also employed to prepare C_3S-gypsum-slag system. A representative X-ray diffraction (XRD) result of C_3S is shown in Fig. 2(a), and the result indicated that it presented a triclinic polymorph. Fig. 2(b) elaborates the XRD scans of these four slags, showing that they were entirely amorphous with no obvious crystal peak.

Table 1
Chemical compositions (wt%) determined by XRF and physical properties of these slags.

	A3	A12	A18	S
CaO	42.07	37.32	36.87	37.40
SiO_2	43.30	39.11	34.43	37.82
Al_2O_3	3.69	12.32	18.19	13.58
MgO	10.83	9.43	7.98	8.11
FeO/Fe_2O_3	0.07	0.30	0.40	0.36
TiO2	–	0.70	0.84	1.22
MnO/Mn_2O_3	–	0.15	0.27	0.30
Na_2O	–	0.24	0.37	–
K_2O	–	0.21	0.41	0.80
SO_3	0.01	0.03	0.03	0.93
LOI[a]	−0.02	−0.03	−0.04	−0.87
Physical properties				
d_{50} (μm)[b]	19.67	20.35	20.85	20.94
SSA (m^2/g)[c]	1.090	0.919	0.904	0.937

[a] The loss-on-ignition (LOI) of slags was determined by thermogravimetric analysis at 950 ± 50 °C. The negative value of LOI is related to the oxidation of sulfur rich species in slag. It should be noted that the LOI value was not corrected in the XRF measurement.
[b] The particle size distribution of slag was measured by EyeTech, Ankersmid. The d_{50} of quartz is 24.21 μm.
[c] The specific surface area (SSA) of slag was measured by nitrogen adsorption with the BET method.

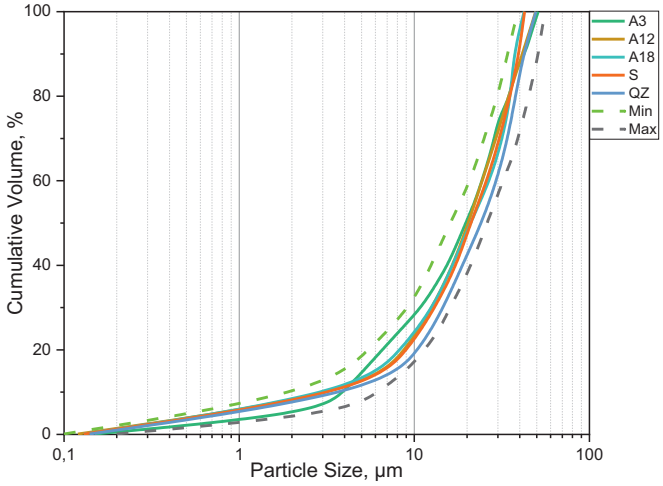

Fig. 1. Particle size distribution of slags and quartz.

2.2. Mix design and experimental method

A summary of the specimens prepared for investigation is listed in Table 2. The slag to C_3S or C_3S + gypsum ratio was 7/3 and the water to binder ratio was 0.4. Sulfate sourcing from gypsum was introduced by replacing C_3S. Each mixture was labelled as their corresponding sulfate content levels, i.e., G0, G1, G3, G5, and G10 for sulfate dosage levels of 0, 1, 3, 5, and 10 wt% of C_3S + gypsum, respectively.

The heat evolution was measured in a TAM Air isothermal calorimeter at 20 °C. Sample was mixed at a high speed for 2 min, ~7 g of the binder was transported to a glass ampoule, sealed and placed in the calorimeter. Paste specimen was prepared in the same manner as the

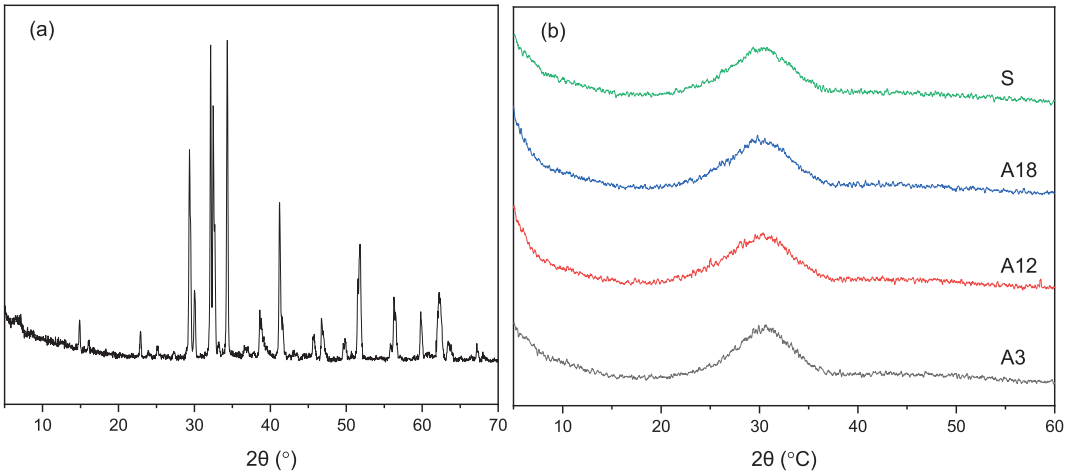

Fig. 2. XRD scan of (a) C_3S and (b) one commercial slag and three synthetic slags used in the present research.

Table 2
Compositions (wt%) of the blends.

	C_3S	Gypsum	Slag	$SO_3/(C_3S$ + gypsum)	Slag/(C_3S + gypsum)
G0	30	0	70	0	7/3
G1	29.355	0.645	70	1 %	7/3
G3	28.065	1.935	70	3 %	7/3
G5	26.775	3.225	70	5 %	7/3
G10	23.550	6.450	70	10 %	7/3

calorimetry measurement, mounted in the plastic bottle of 20 mL and sealed with thin para film on the seal to avoid any ingression of carbon dioxide and evaporation of vapor. Sealed curing was performed for all specimens at 20 ± 3 °C for 1 day and 3 days before any measurements.

For XRD measurement and thermogravimetric analysis (TGA), the continuous hydration of specimen was stopped by solvent exchange with isopropanol. Slices of specimen were cut, crushed, and ground to below 63 μm. X-ray powder diffraction was performed on a Philips PW 1830/40 Powder diffractometer employing the Cu K-alpha radiation. The machine was operated with an acceleration voltage of 40 kV and an X-ray beam current of 40 mA. Analysis was performed with a step size of 0.03° and for a 2θ range from 5° to 60°. Thermogravimetric analysis was carried out by Netzsch STA 449 F3 Jupiter under Argon atmosphere. Approximately 50 mg of the material was heated from 40 to 900 °C with a heating rate of 10 °C/min in an Al_2O_3 crucible with an identical crucible as reference.

Meanwhile, the fresh fracture surface of specimen was observed with a FEI QUANTA FEG 650 ESEM in secondary electron (SE) mode after hydration stop. Moreover, the overall development of microstructure was observed on the polished surface in backscattered electron (BSE) mode. To get BSE images, slices of hydrated specimen were cut, immediately immersed in isopropanol solution for hydration stop, dried at 40 °C subsequently, impregnated with epoxy resin and polished down to 0.25 μm. X-ray energy dispersive (EDS) detector was used to determine the elemental composition of hydrate assemblage. All microanalysis was carried out in high vacuum chamber condition at a working distance of 10 mm and an accelerating voltage of 15 kV.

3. Results and discussions

3.1. General pattern of the reaction of C_3S-gypsum-slag system

Fig. 3 illustrates the heat flow and heat release of C_3S-5 wt% gypsum-slag system (G5), normalized to per gram of C_3S. The heat flow was dominated by one main peak occurring at about 10 h after mixing, associated with the hydration of C_3S, and followed by a hump after 1 day (labelled A), which was affected by the amount of Al_2O_3 in slag and gypsum content added. This hump was indicative of secondary reaction between Al^{3+} ion from slag and SO_4^{2-} ion from gypsum.

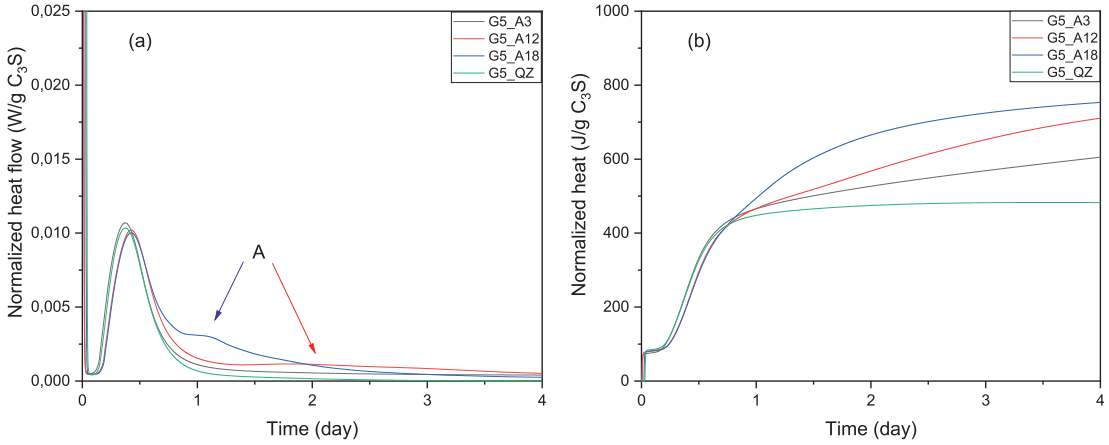

Fig. 3. (a) Heat flow and (b) total heat release as a function of time in calorimetric measurement for C_3S-5 wt% gypsum-slag system. As seen in (b), the heat release before 1 day was almost the same irrespective of the Al_2O_3 content of slag.

3.1.1. Effect of Al_2O_3 in slag

It is well recognized that Al^{3+} ion has a perturbing effect on the reactivity of silicate [23–27], relying mainly on aluminate concentration and pH of the solution [26,27]. As seen in the present research (Fig. 4 (a)), when increasing Al_2O_3 content in slag, the induction period became longer, implying a rough dependence on alumina dosage. Surface poisoning is believed to take place either through covalent bonding between alumina and silicate on the surface or through the adsorption of alumina on the etch pits [27]. Another mechanism that has been put forward is the negative effect of alumina on the nucleation and growth of silicate hydrates [6,28]. Moreover, compared with C_3S-quartz blend, a small decrease in the rate of heat flow (slope) during acceleration period and the intensity of main hydration peak was observed, with the presence of alumina. The more Al_2O_3, the more drop. It was in contrast with the results from [29], which concluded that the intensity of main peak and total heat release increased with increasing Al^{3+} ion concentration, indicating a higher hydration degree of C_3S. On the other hand, the deceleration period appeared to be unaffected by the presence of Al_2O_3.

3.1.2. Effect of gypsum

As shown in Fig. 4(b), gypsum itself seemed to exert few impact on the hydration of C_3S when compared in C_3S-quartz-gypsum mixture. The rate of heat flow during acceleration and deceleration period was nearly the same when different amounts of gypsum were added, except for a small variation of the main peak intensity. It was consistent with the results from [6], where the reaction rate of C_3S with or without gypsum addition was almost identical. Additionally, the dormant period ended a little earlier with gypsum, indicating that SO_4^{2-} ion increased the deviation of C_3S from the solubility equilibrium, and its dissolution was accelerated accordingly [26].

3.1.3. Effect of Al_2O_3 and gypsum together

It was different when slag and gypsum were added together into the system. As seen in Fig. 5(a), for C_3S-gypsum-slag A3 system, the hydration process was accelerated, proved by the shortened induction period even compared with C_3S-quartz blend. Al^{3+} ion absorbed on the reactive site of C_3S was removed by SO_4^{2-} ion immediately, and as mentioned earlier, the rest SO_4^{2-} ion increased the deviation of C_3S from the solubility equilibrium. The hydration of C_3S was thus accelerated. Besides, it should be noted that the interaction between Al^{3+} and SO_4^{2-} ions led to the formation of ettringite through the equation below. Its precipitation decreased the concentration of Ca^{2+} in the pore solution, and increased the undersaturation levels with respect to C–S–H gel phase and portlandite. Therefore, C_3S-gypsum-slag A3 system entered into acceleration period firstly.

$$6Ca^{2+} + 2AlO_2^- + 3SO_4^{2-} + 4OH^- + 30H_2O \rightarrow Ca_6Al_2(SO_4)_3(OH)_{12}\cdot 26H_2O$$

Similarly, for C_3S-gypsum-slag A12 and A18 systems, the induction period also ended earlier than C_3S-slag A12 and A18 systems without gypsum, but a little later than C_3S-quartz blend (Fig. 5(b) and (c)). When increasing gypsum addition from 1 to 10 wt%, it made few differences. Apparently, the Al^{3+} concentrations in the pore solution of slag A12 and A18 were higher than that in slag A3 due to their higher Al_2O_3 contents in slag. Probably SO_4^{2-} ion provided by gypsum cannot combine all Al^{3+} ion absorbed on the C_3S surface in time, and residual Al^{3+} ions were still absorbed on the C_3S surface. For this phenomenon, it deserves further research.

3.2. Second reaction peak (aluminate peak)

For pure cement system, the second reaction peak originates from the renewed reaction between C_3A and sulfate, and the work in [8,30] found that the peak was delayed and became broader with increasing additional gypsum content. Also, this peak may not be well visible in the calorimetry curve as it is often present as a low and broad peak. Nonetheless, this peak occurred in C_3S-gypsum-slag mixture in the present research with the absence of C_3A (see Fig. 6), and was associated with the Al_2O_3 content of slag and gypsum content added remarkably.

In a properly sulfated cement system, the second aluminate peak in calorimetry measurement occurs right after the main hydration peak. All the mixtures investigated in the article belong to this case. However, in a undersulfated system, a large and sharp peak, related to the formation of calcium monosulfoaluminate (monosulfate for short), occurs much earlier before the main hydration peak, and the reaction of C_3S is delayed and suppressed [6,31]. This is not the case in the present research even with only 1 wt% gypsum addition (G1) owing to the reactivity of slag, which is much inferior to C_3A. As for oversulfate system, more retardation on the reaction of C_3A can be observed [4].

3.2.1. Parameters controlling the hydration kinetics of aluminate reaction

As Fig. 6(a) illustrates, after the main hydration peak, the heat evolution was featured by a period when the reaction was accelerated to a small peak and then slowed down, especially for those with high gypsum addition. The second reaction peak in C_3S-gypsum-slag A18 system started to be visible when 5 wt% gypsum was added and a little delayed when increasing gypsum content from 5 to 10 wt%.

It was also noticed that the onset of aluminate peak (beginning of the deviation from C_3S-quartz blend) occurred at a similar timing (~15 h after mixing as Fig. 6(a) presents) or cumulative heat release (~400 J/(g

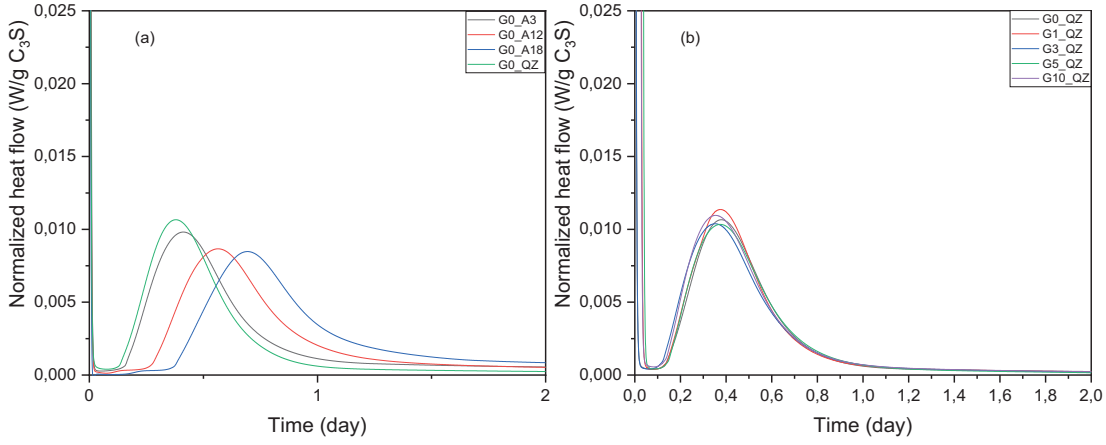

Fig. 4. (a) The dormant period or the nucleation of C_3S was strongly modified in the presence of slag containing different Al_2O_3 contents. (b) The reaction rate of pure C_3S with or without gypsum addition was almost identical.

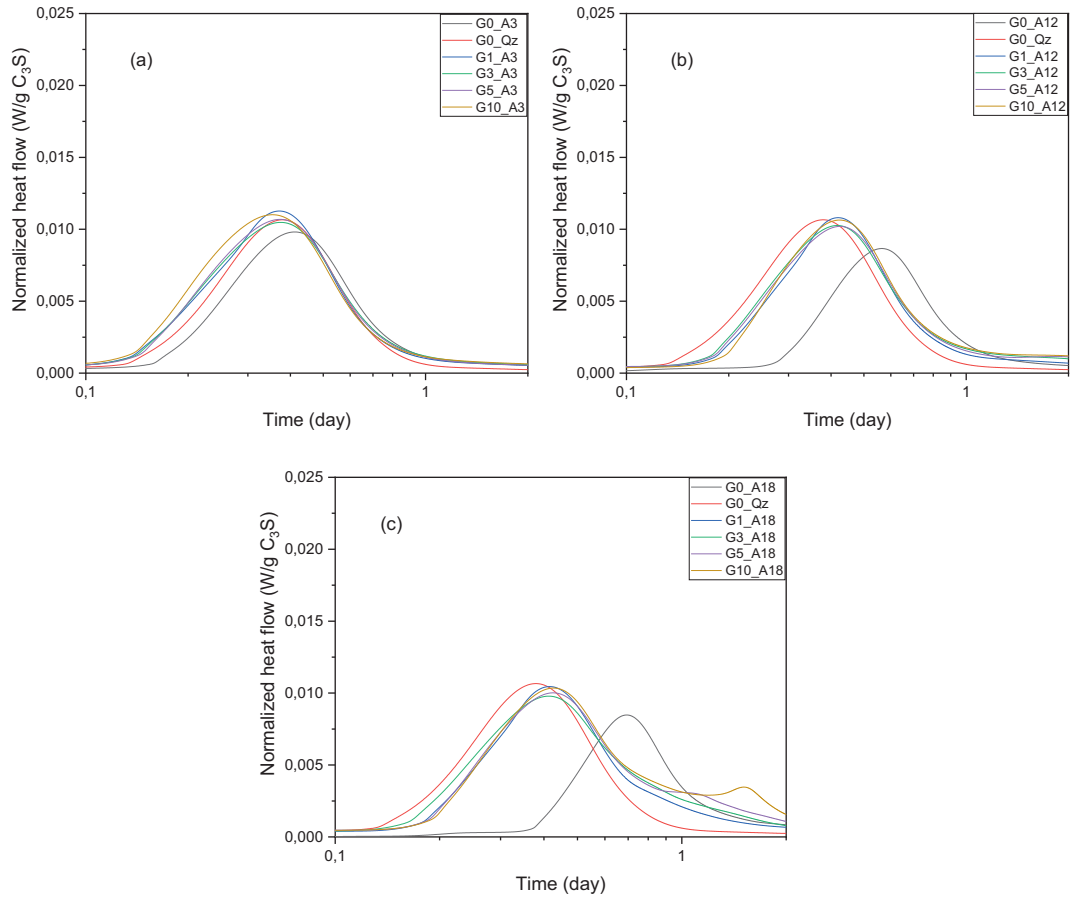

Fig. 5. Calorimetric curves of C_3S-slag blend with different gypsum additions. (a) The addition of gypsum promoted the earlier end of induction period in C_3S-slag A3 blend compared with C_3S-quartz blend; As for C_3S-gypsum-slag A12 (b) and A18 (c) systems, the induction period ended a little later than C_3S-quartz blend. These curves were plotted on log scale to highlight the difference at early age.

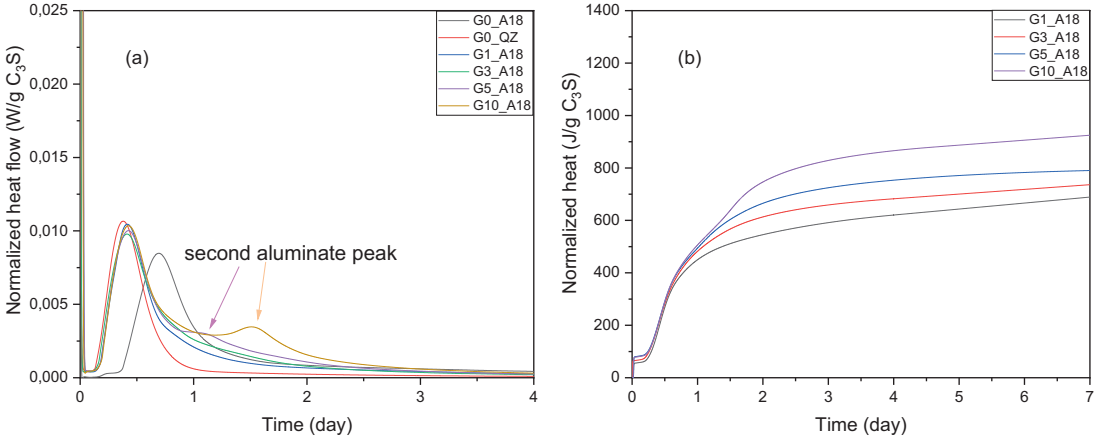

Fig. 6. Calorimetric curves of C_3S-slag A18 blend with different gypsum additions. (a) The aluminate peak was delayed, and became more visible with the increasing gypsum addition; (b) The normalized heat release curves were almost identical before ~15 h (about ~400 J/g C_3S) after mixing, and they separated from each other from then on.

C_3S) as Fig. 6(b) presents) for all mixtures irrespective of the amount of gypsum added. The heat was mainly released by silicate reaction until this timing, i.e., the hydration of C_3S, which suggested that the onset of aluminate reaction also depended on silicate reaction, perhaps the production of enough C−S−H gel phase to absorb sulfate. Zunino, F. et al. [19] concluded that the heat release before aluminate peak was directly related to the content of gypsum added and the fineness of C_3A, in other words, it was determined by the amount of silicate reaction and ettringite formation. In the present research where there was no C_3A in the mixture, the almost same heat release before aluminate peak demonstrated that the precipitation of ettringite was very few even in G10_A18 mixture. It proved indirectly that SO_4^{2-} ions cannot combine all Al^{3+} ions absorbed on the C_3S particle surface during the induction period (Section 3.1.3).

For systems with lower Al_2O_3 content in slag, this period was almost invisible (slag A3 in Fig. 7(a)) or characterized by a hump (slag A12 in Fig. 7(b)). Therefore, it was assumed that the aluminate reaction was controlled by the availability of reactants, SO_4^{2-} and Al^{3+} ions in particular for the formation of ettringite. Nuclei of ettringite precipitate and grow at a rate proportional to the concentrations of SO_4^{2-} and Al^{3+} ions [32,33].

Fig. 8(a) presents the normalized heat release of C_3S-gypsum-slag A3 system until 4 days with different gypsum additions. The shape of curve was analogous to each other and the difference of total heat release was very small among each other. Hence it was convincible to conclude that the amount of gypsum added was adequate to react with Al^{3+} ion in each mixture, and the availability of Al^{3+} ion was the rate-controlling factor. Fig. 8(b) and (c) illustrate the normalized heat release of C_3S-3 and 5 wt % gypsum-slag systems (G3 and G5). It was noted that although the total heat releases of slag A12 and A18 mixtures were different until 4 days, it coincided with each other after 7 days of curing. It implied that the same amount of reaction occurred in slag A12 and A18 mixtures until 7 days, whereas the kinetics were different and affected by the availability of reactants. There seemed to be abundant Al^{3+} ions in these two mixtures to participate into the aluminate reaction. Thus, the availability of SO_4^{2-} ion was the rate-controlling factor for slag A12 and A18 systems when gypsum addition was <5 wt%. Fig. 8(d) shows the normalized heat release of C_3S-10 wt% gypsum-slag system (G10) until 7 days. The difference of total heat release between slag A12 and A18 mixtures became evident, indicating that SO_4^{2-} ion was sufficient in the pore solution and the availability of Al^{3+} ion dominated the reaction again. The rate-controlling factor of aluminate reaction in each run is summarized in the Table 3.

Moreover, it was noticed that all cumulative heat release curves deviated from each other at a similar timing, i.e., ~15 h after mixing or ~400 J/(g C_3S) as displayed from Fig. 8(a) to (d). The same heat release before the onset of aluminate peak further confirmed that the precipitation of ettringite was few in all mixtures, irrespective of alumina content in slag. On the other hand, it indicated that the dissolution degree of slag before one day was very low, and the surface area of slag could be considered to be unchanged at this stage. After one day, slag, especially with high alumina content, could not be regarded as inert filler any more, and it took part into the aluminate reaction with gypsum significantly.

Another aspect needed to be emphasized was the location where ettringite grew, on the surface of C_3S particle, slag particle or in the pore solution. Firstly, it was unlikely for ettringite to nucleate and grow on the surface of C_3S particles as their surface had been occupied by C–S–H gel phase after main hydration peak (Fig. 15). Moreover, as Fig. 14 shows, these needle-like ettringite was more likely to grow from the pore solution with an exclusive through-solution formation, as reported in [32].

3.2.2. *Heat release from aluminate reaction vs. SO_3 and Al_2O_3 contents of the mixture*

Fig. 9(a) and (b) display the heat release from aluminate reaction against SO_3 content of gypsum and Al_2O_3 content of slag, respectively. An approximatively linear correlation between SO_3 content and heat release from aluminate reaction, taken as an indication of the amount of ettringite formed, is found and depicted in Fig. 9(a). A linear function was selected for fitting, and its parameters were determined by the least-square method considering all points investigated. For slag A3 and A12 systems, slopes were in direct proportion to their corresponding Al_2O_3 contents, while for slag A18 system, the slope was a little higher compared to its Al_2O_3 content, i.e., $3.75/3.69 \approx 10.99/12.32 < 23.51/18.19$. The roughly linear correlation was also found between Al_2O_3 content of slag and heat release in most mixtures investigated (Fig. 9(b)), except for C_3S-10 wt% gypsum-slag A18 mixture, which presented a significant high heat release from aluminate reaction. Unlike alumina in slag A3 and A12 systems only participating into the formation of ettringite, aluminum dissolved from slag A18 played role both in the formation of ettringite and monosulfate (see discussion in Section 3.3.1). The heat evolved from the transformation from ettringite to monosulfate in slag A18 mixture was also included in the aluminate reaction without differentiation. As a result, more heat and higher slope were determined in this mixture.

3.2.3. *Effect of sulfur rich species of slag*

The sulfur rich species of slag mainly sources from iron pyrite used as raw material and fuel for energy. It exists as anion S^{2-} in the molten slag liquid due to the reduction condition in the blast furnace [34,35]. During quenching, it will be emitted in the form of H_2S with water vapor. The rest exists as sulfide (e.g., CaS) in slag, whereas its amount is presented in the form of SO_3 by XRF. In the pore solution of slag cement paste, dissolved S^{2-} ion could be readily oxidized depending on oxygen diffusion into pores through thiosulfate ($S_2O_3^{2-}$) to most stable sulfate (SO_4^{2-}) [36,37].

As shown in Fig. 10, it was found that the sulfur rich species incorporated in commercial slag exerted a key impact on the hydration of C_3S-slag S blend when without gypsum addition. On the one hand, the dormant period ended earlier in C_3S-slag S mixture compared with that in C_3S-slag A12 mixture (Slag A12 contained nearly no sulfur (see LOI value in Table 1)). In addition, the heat flow curve of C_3S-slag S mixture was almost identical with that of C_3S-3 wt% gypsum-slag A12 mixture, especially for the similar duration of induction period. It suggested that the sulfur species in slag S acted the same role as sulfate dissolved from

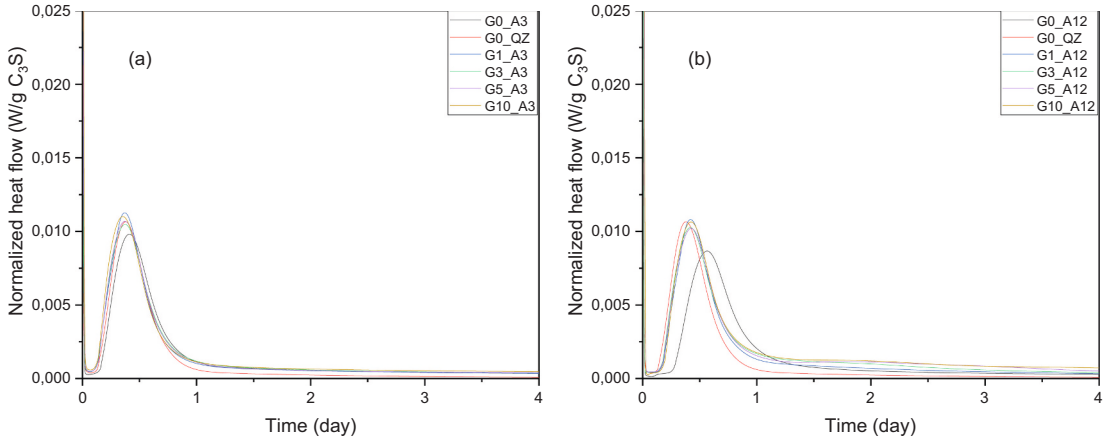

Fig. 7. Calorimetric curves of C_3S-slag (a) A3 and (b) A12 blends with different gypsum additions. The aluminate peak was invisible in slag A3 system or characterized by a hump in slag A12 system.

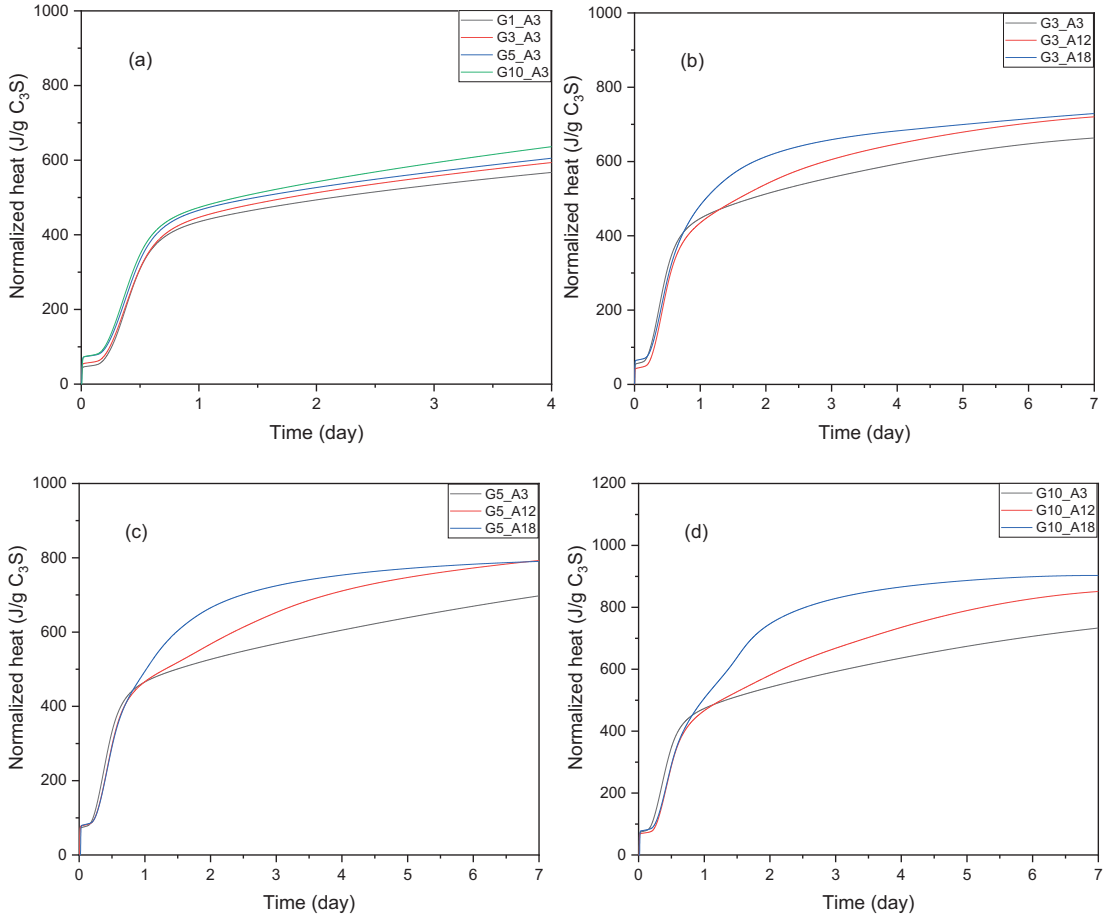

Fig. 8. (a) Hear release of C_3S-gypsum-slag A3 system and the availability of Al^{3+} ion in the pore solution was the rate-controlling factor in this system; (b) and (c) Heat release of C_3S-3 and 5 wt% gypsum-slag systems respectively, and there seemed to be abundant Al^{3+} ions to participate into the aluminate reaction and the availability of SO_4^{2-} ion was the rate-controlling factor; (d) Heat release of C_3S-10 wt% gypsum-slag system and the availability of Al^{3+} ion dominated the reaction again as SO_4^{2-} ion was sufficient in the pore solution.

Table 3
The rate-controlling factor of aluminate reaction in each run, the availability of Al^{3+} or SO_4^{2-} ion.

	A3	A12	A18
G1	Al^{3+}	SO_4^{2-}	SO_4^{2-}
G3	Al^{3+}	SO_4^{2-}	SO_4^{2-}
G5	Al^{3+}	SO_4^{2-}	SO_4^{2-}
G10	Al^{3+}	Al^{3+}	Al^{3+}

gypsum, and Al^{3+} ion absorbed on the reactive site of C_3S would be removed by SO^{4-} ion transformed from sulfur species. On the other hand, the hump (labelled as A) indicating the reaction between Al^{3+} and SO^{4-} ions for the formation of ettringite was also noted in the C_3S-slag S mixture.

To semi-quantify the effect of sulfur species incorporated in commercial slag S, calorimetric measurement of C_3S-slag A12 and S systems with different gypsum additions is compared in Fig. 11. The duration of induction period, the rate of heat flow during acceleration and deceleration period, and the occurrence of main hydration peak were nearly the same in these mixtures, except for a small variation of the main hydration peak intensity (Fig. 11(a)). As for the cumulative heat release, it was noted that C_3S-3 and 5 wt% gypsum-slag A12 mixtures presented almost the same heat as C_3S-1 and 3 wt% gypsum-slag S mixtures up to 4 days, respectively. In other words, about 2 wt% of gypsum was added into the blend by commercial slag S additionally through sulfur rich species.

3.3. Hydration products

3.3.1. Solid phase

DTG results of typical mixtures are displayed in Fig. 12. The main hydrates formed in the mixture without gypsum were similar (Fig. 12 (a)). The mass loss from 400 to 500 °C was sourced from the dehydration of portlandite. Hydrotalcite-like phase can also be detected (mass loss at around 350 °C). The mass loss at ~150 °C indicated the presence of C−S−H gel phase. More hydrates were identified with hydration, and compared with C_3S-quartz mixture, more C−S−H gel phase while less portlandite were detected in C_3S-slag mixture as part of portlandite and slag was consumed in pozzolanic reaction for the secondary precipitation of C−S−H gel phase and hydrotalcite-like phase.

For C_3S-gypsum-slag system (Fig. 12(b)), apart from phases identified earlier, ettringite was observed as the peak at ~150 °C became narrow and shifted left a little bit (Fig. 12(c)). Furthermore, monosulfate occurred in slag A18 mixture from the first day. Compared with C_3S-gypsum 5 wt%-slag A3 paste, slag A18 paste produced more ettringite + C−S−H gel phase and monosulfate (only visible in slag A18 paste) after 3 days of curing. Meanwhile, less portlandite was identified in slag A18 mixture due to its consumption in the formation of ettringite with gypsum and transformation from ettringite to monosulfate.

XRD scans (Fig. 13) reveal the presence of portlandite and unhydrated C_3S in the pastes. For C−S−H gel phase, the main peaks are located at ~30° (2θ) (PDF 34−0002 and PDF 34−0306), which is very difficult to distinguish from that of C_3S. It was also evidenced that monosulfate started to be detected in slag A18 paste containing gypsum

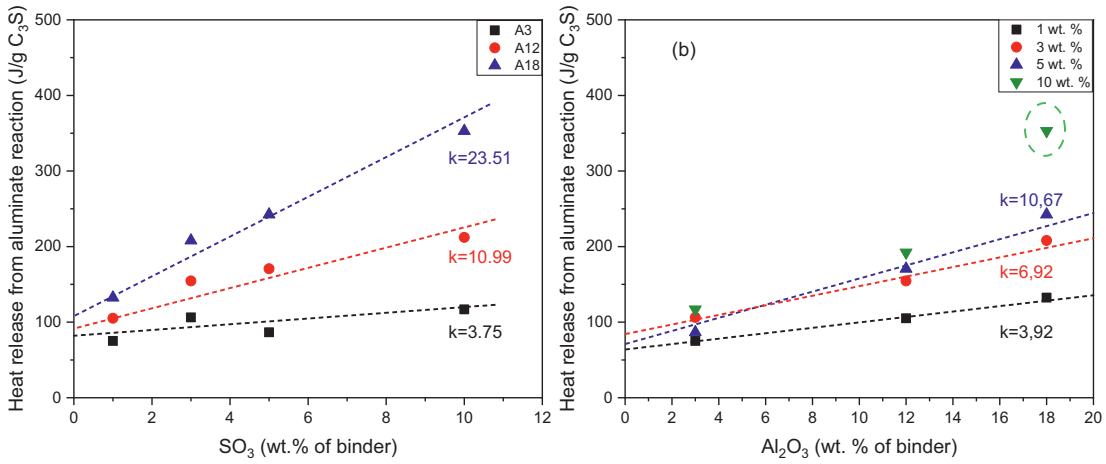

Fig. 9. Heat release from aluminate reaction against (a) SO_3 content of gypsum and (b) Al_2O_3 content of slag.

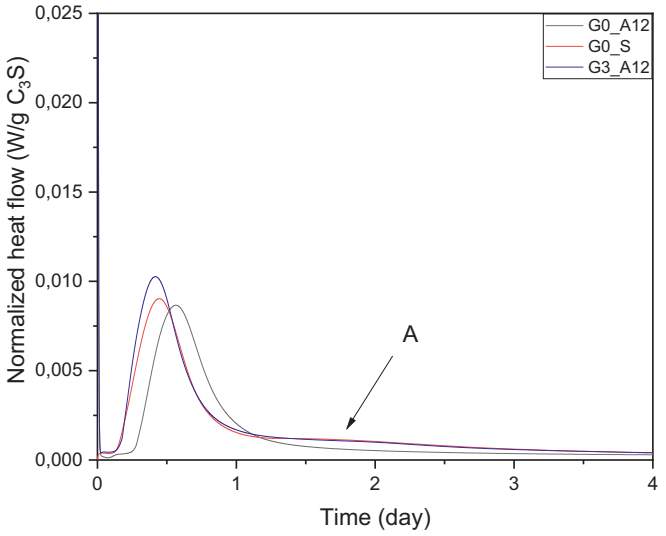

Fig. 10. Heat flow as a function of time in calorimetric measurement for C_3S-slag A12 and S systems.

from the first day (Fig. 13(c)), and the transformation from ettringite to monosulfate proceeded continuously with hydration. It deserved to mention that there was no monosulfate detected either by TGA or XRD in C_3S-gypsum 5 wt%-slag A3 and A12 systems.

3.3.2. *Microstructure*

Fig. 14 illustrates the representative BSE image of C_3S-5 wt% gypsum-slag A18 system after 3 days of curing. The mixture of anhydrous materials, hydrated phases and pores was clearly visible. Small C_3S grains, or so-called Hadley grains, hydrated completely after 3 days to leave hollow hydration shells (circled and labelled as 1). Large C_3S grains continued to hydrate, and there was a clear grey level difference between the outer products (Op) appearing dark grey, and more dense products (Ip) appearing light grey around unhydrated C_3S particle (circled and labelled as 2). Mass of ettringite (long needle shape) was observed frequently and crystallized in or near pores. Monosulfate only existed in slag A18 paste as fine and compact crystal intermixed with C–S–H gel phase (circled and labelled as 3). Although slag hydrated slowly, the formation of hydrates around unhydrated slag particles were observed (circled and labelled as 4).

Fig. 15(a) and (b) display the morphology of hydrates in C_3S-slag A12 mixture without gypsum at 3 days, where (a) clearly elaborates the precipitation of C–S–H gel phase and portlandite on the surface of slag particle. As shown in (b), hexagonal thin plates of portlandite were identified intermixed with C–S–H gel phase closely. It was also noticed that converging needles rather than a divergent fibrillary-like structure

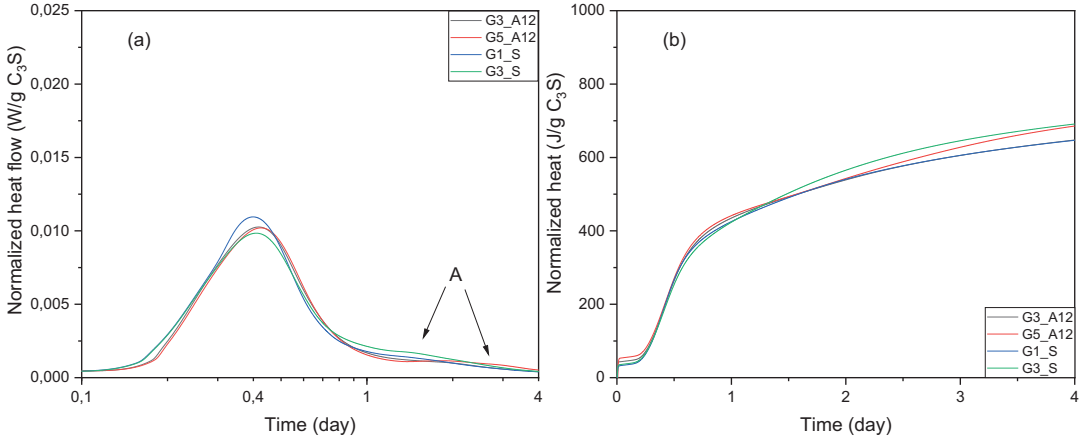

Fig. 11. (a) Heat flow and (b) total heat release as a function of time in calorimetric measurement for C_3S-slag A12 and S systems with different gypsum additions. (a) was plotted on log scale.

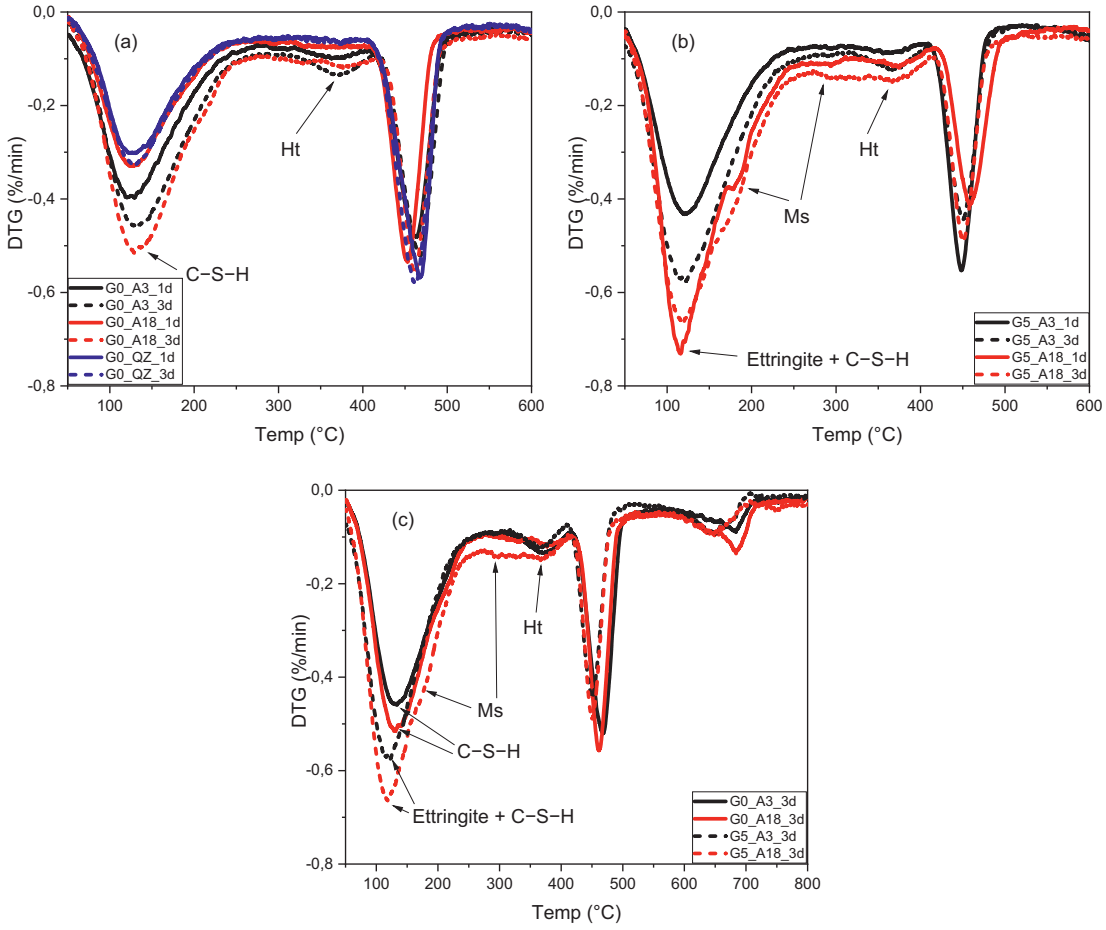

Fig. 12. Exemplary results of DTG analysis of paste (a) without gypsum and (b) with gypsum after 1 and 3 days of curing; (c) comparison between them. Ms: calcium monosulfoaluminate; Ht: hydrotalcite-like phase.

of C−S−H gel phase was seen in mixtures without gypsum at the very beginning of reaction. It was consistent with the results in [38], which confirmed that it was the pore solution chemistry, like the existence of SO_4^{2-} ion, changed the morphology of C−S−H gel phase by promoting repulsion between the growing structure. Fig. 15(c) illustrates the morphology of hydrates in C_3S-gypsum 5 wt%-slag A12 mixture at 3 days. Besides C−S−H gel phase and portlandite, the long needle crystal indicated the formation of ettringite in the system with gypsum. Also, a divergent fibrillary-like structure of C−S−H gel phase was observed due to the introduction of gypsum [38].

3.3.3. *Chemical composition of C−S−H gel phase*

The chemical composition of C−S−H gel phase of investigated mixtures detected by SEM-EDS point analysis is shown in Fig. 16. It should be noted that the two different types of C−S−H gel phase, i.e., inner product (IP) and outer product (OP) were not distinguished in the present paper. The Si/Ca atomic ratio of C−S−H gel phase varied from 0.4 to 1.2 in both C_3S-slag A3 and A18 mixtures without gypsum. The trend of Al/Ca atomic ratio was also similar, the majority of which was <0.1. Thus, the Ca/Si and Al/Si atomic ratios of C−S−H gel phase formed in mixtures without gypsum seemed to be independent of Al_2O_3 content of slag.

For mixtures with gypsum, the Si/Ca atomic ratio of C−S−H gel phase fluctuated a little bit, still varying from 0.4 to 1.2. However, significant more Al in the matrix was observed in these two mixtures. When there was attraction from sulfate, besides that fixed in hydrotalcite-like phase, the rest Al^{3+} ions would enter into the matrix, either take part in the formation of ettringite or be absorbed into C−S(A)−H gel phase, resulting in a higher Al/Si ratio. On the other hand, it was also pointed out in [39] that the degree of polymerization of C−S−H gel phase at this early age may not be sufficient for Al to be accommodated within the structure. At least, it was more likely that the aluminum existed in ettringite and/or monosulfate layers intermixed with C−S−H gel phase layers.

3.4. *Thermodynamic modelling*

To verify the results of the above measurements, thermodynamic modelling was carried out using the Gibbs free energy minimization program GEMS [40,41] with thermodynamic data from the PSI-GEMS database [42,43] supplemented by cement specific data [44,45]. The calcium-alkali aluminosilicate hydrate ideal solid solution model (CNASH_ss) proposed by Myers et al. [46] was employed to describe the C−A−S−H gel phase in the system. MA-OH-LDH_ss containing three end-members with Mg/Al ratios of 2, 3 and 4 reformulated into an ideal solid solution was used to perform the modelling of hydrotalcite–like solid solution series [47]. For simplicity, some assumptions were introduced. For example, reactants of different hydration degrees were assumed, and it was postulated that slag dissolved congruently. The used hydration degree was 80 % for C_3S, 100 % for gypsum, and 15 % for slag at 3 days. Moreover, the modelling did not consider the difference of hydration degree among slags, and it only reflected equilibrium phase assemblage accounting for thermodynamic approach.

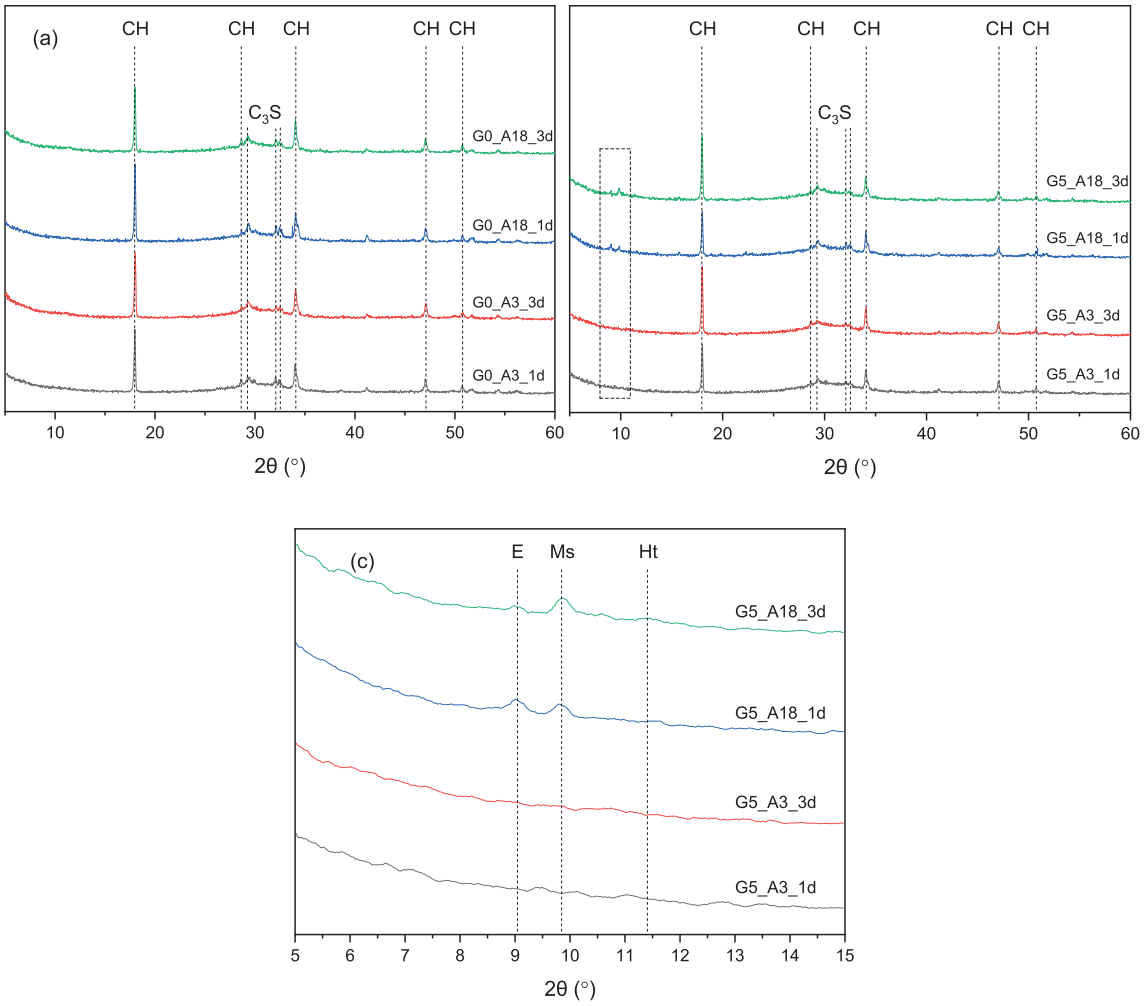

Fig. 13. Exemplary results of XRD analysis of specimens (a) without gypsum (b) with gypsum at 1 and 3 days; (c) zoom in the rectangle area from 5 to 15° (2θ) in (b). CH: portlandite; E: ettringite; Ms: calcium monosulfoaluminate; Ht: hydrotalcite-like phase.

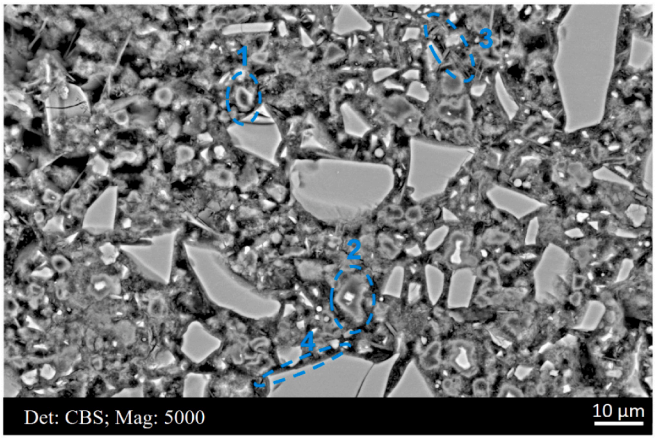

Fig. 14. Microstructure of C_3S-5 wt% gypsum-slag A18 blend after 3 days of curing. 1: Hadley grain and hollow hydration shell was formed; 2: a clear grey level difference between the outer product and inner product formed around partially hydrated C_3S grain; 3: fine and compact crystal of monosulfate; 4: hydrates formed around partially hydrated slag particle.

3.4.1. *Effect of Al_2O_3 content of slag*

Fig. 17 elaborates the impact of Al_2O_3 content in slag on the volume of phase assemblage with 5 wt% gypsum addition. Increasing Al_2O_3 content from 3.69 (slag A3) to 18.19 wt% (slag A18) firstly increased the amount of ettringite formed until the consumption of gypsum (labelled as point P1 in the graph). Then, ettringite content stabilized with the continuous increase of Al_2O_3 content until the transformation from ettringite to monosulfate started (labelled as point P2 in the graph.). For slag with few Al_2O_3, it was supposed that all Mg^{2+} ion dissolved from slag was bound into magnesium silicate hydrate (M−S−H) rather than brucite ($Mg(OH)_2$) owing to its low diffusion ability [48,49], and when adequate Al_2O_3 content was accumulated, all magnesium entered into hydrotalcite-like phase due to its lower solubility product (Ksp) compared with M−S−H.

Gypsum was surplus when slag contained few Al_2O_3 as revealed in the modelling, which was consistent with the results shown in Fig. 8(a), and it was thus concluded that for C_3S-gypsum-slag A3 blend, gypsum was sufficient to react with Al^{3+} ion dissolved from slag. As for slag A12 and A18 blends, the availability of gypsum was the rate-controlling factor. The results from modelling were also in agreement with the change of phase assemblage reflected by TGA (Fig. 12) and XRD (Fig. 13). The formation of monosulfate became increasingly prominent with additional Al_2O_3 content. It was also noted that the portlandite content decreased significantly upon the occurrence of monosulfate. These results verified the following equation for the formation of monosulfate involving the participate of ettringite, portlandite, and aluminate dissolved from slag, i.e.,

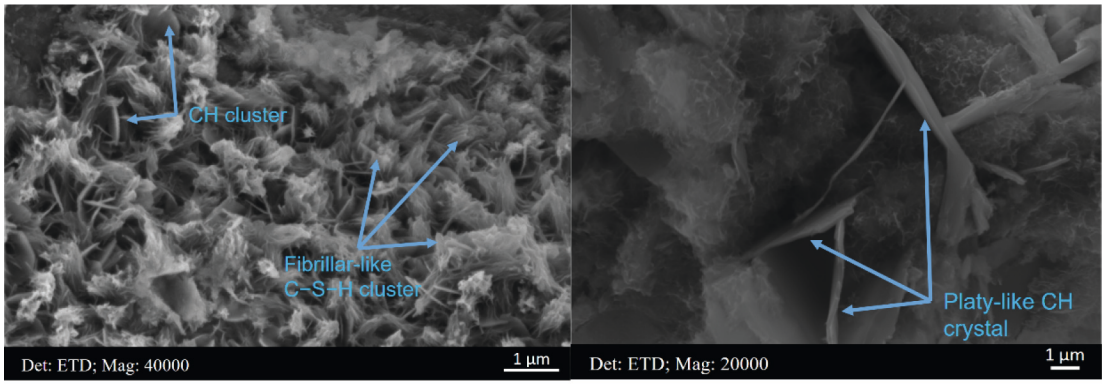

(a) (b)

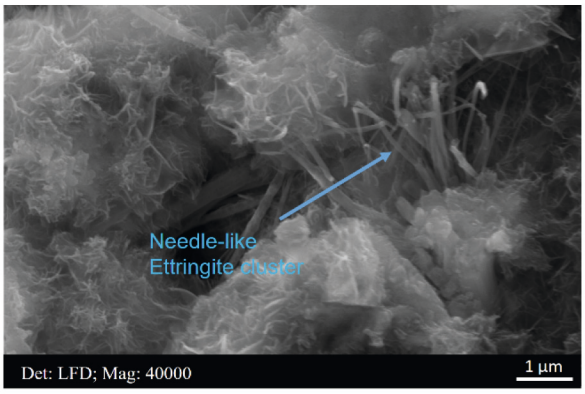

(c)

Fig. 15. Morphology of different hydrates of (a) and (b) C_3S-slag A12 blend at 3 days; (c) C_3S-5 wt% gypsum-slag A12 blend at 3 days. CH: portlandite.

$$Ca_6Al_2(SO_4)_3(OH)_{12}\cdot 26H_2O + 6Ca(OH)_2 + 4AlO_2^- + 4H^+ \rightarrow 3Ca_4Al_2(SO_4)(OH)_{12}\cdot 6H_2O + 4H_2O$$

3.4.2. *Effect of gypsum*

Fig. 18 elaborates the impact of gypsum addition on the phase assemblage based on C_3S-gypsum-slag A18 blend. The volume of monosulfate increased gradually at the beginning when alumina dissolved from slag was sufficient, and it prevented the formation of ettringite; however, ettringite started to occur with the continuous addition of gypsum (labelled as point P in the graph), implying that adequate sulfate favored the precipitation of ettringite.

It was important to note that the stabilization of ettringite with the addition of extra sulfate led to a remarkable increase in the volume of hydrates. Before point P circled in the graph, the total volume changed slightly, whereas it increased apparently with the formation of ettringite although the volumes of C–S–H gel phase and monosulfate decreased. This phase contributes a lot to space filling [51].

Collectively, dependent of the alumina content of slag and gypsum content added, aluminum dissolved from slag contributed to the aluminate reaction significantly. Therefore, when calculating SO_3/Al_2O_3 ratio, alumina content of slag should also be taken into consideration. Especially for slag with high Al_2O_3 content (slag A18 in this paper), approximately 8 wt% of gypsum was requested to maximum the amount of ettringite that can be produced at 3 days. Meanwhile, the sulfur species in commercial slag acted a similar role as sulfate dissolved from gypsum. In the following research, the authors would extend the C_3S-gypsum-slag system to C_3S-C_3A-gypsum-slag system, and compare it with real cement-slag system, to promote the understanding of hydration characteristics of slag-rich cement paste at early age.

4. Conclusions

The present research investigated the hydration characteristics of C_3S-gypsum-slag system at early age. As shown above, the interaction among C_3S, sulfate (gypsum) and Al_2O_3 (slag) was complex, and conclusions were mainly obtained based on aluminate reaction:

- Al^{3+} had a perturbing effect on the reactivity of silicate, and the more Al_2O_3 in slag, the longer of induction period. Gypsum itself had little impact on the hydration of C_3S; however, when slag and gypsum were added together into the system, the duration of dormant period was reduced.
- The onset of aluminate peak in the calorimetric curve occurred at a similar timing (~15 h after mixing) or cumulative heat release (~400 J/g C_3S) for all mixtures irrespective of the amount of Al_2O_3 in slag and gypsum content added.

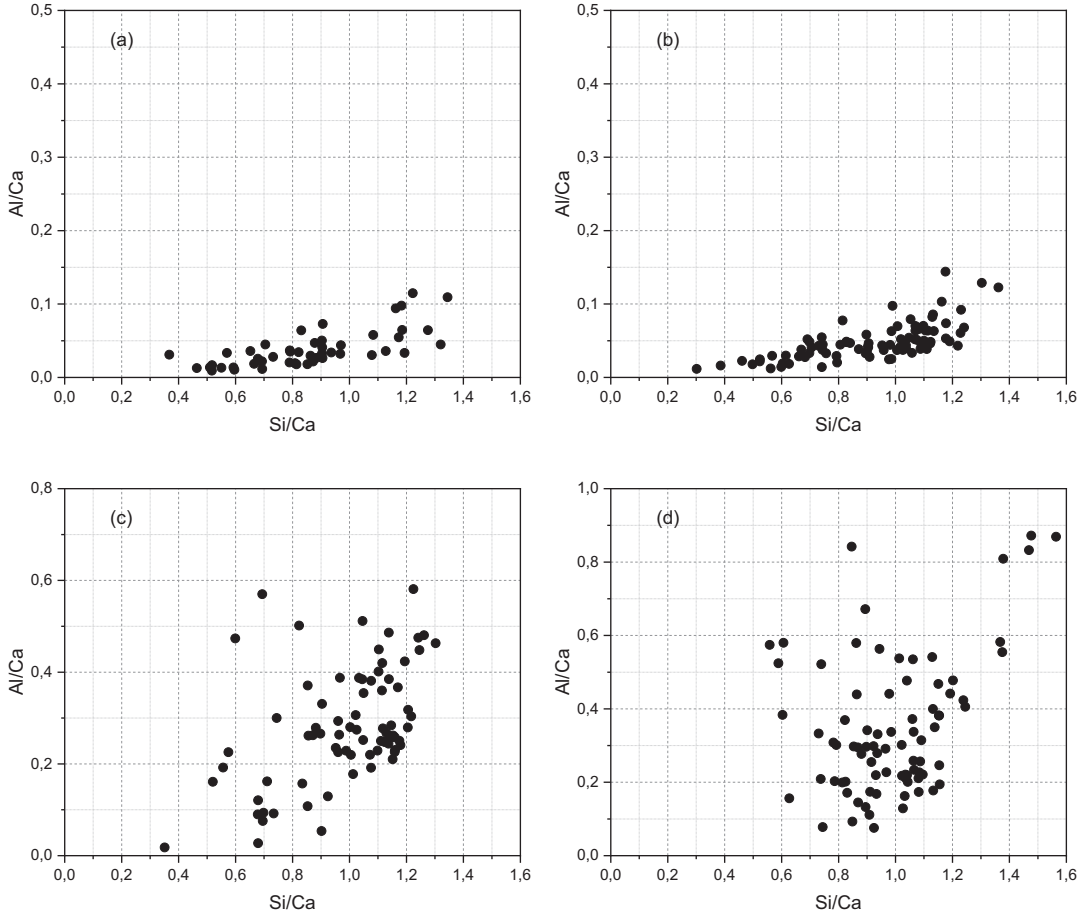

Fig. 16. Atomic ratio of Al/Ca against Si/Ca of (a) and (b) C_3S-slag A3 and A18 mixtures, respectively at 3 days; (c) and (d) C_3S-5 wt% gypsum-slag A3 and A18 mixtures, respectively at 3 days.

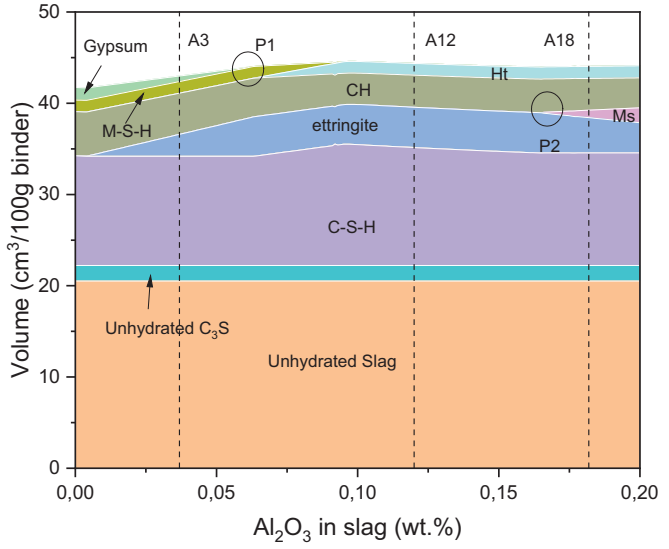

Fig. 17. Changes in the total volume of hydrates as an effect of Al_2O_3 content of slag after 3 days of hydration. The dash lines represent three synthetic slag levels that were investigated in the present study. C_3S-5 wt% gypsum-slag system was considered here. The hydration degree of C_3S was calculated based on calorimetric measurement, and the hydration degree of slag was obtained based on a simple selective dissolution test [50]. Volume expressed as cm^3/100 g unhydrated binder. CH: portlandite; Ht: hydrotalcite-like phase; Ms: calcium monosulfoaluminate.

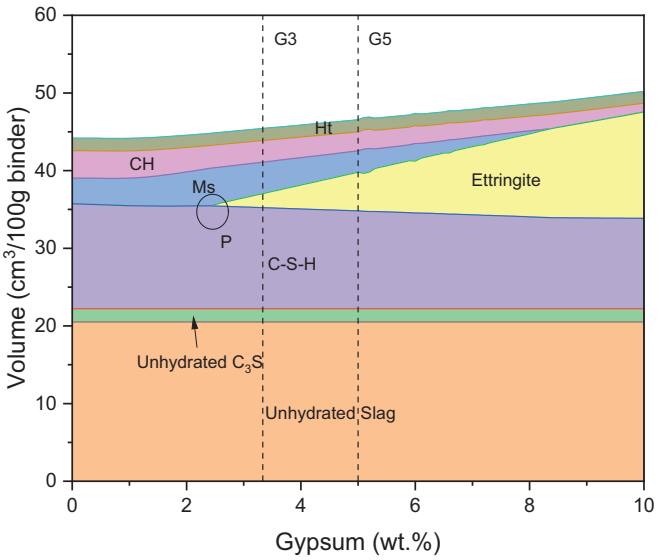

Fig. 18. Changes in the total volume of hydrates as an effect of gypsum content after 3 days of hydration. The chemical composition of slag A18 was employed in the modelling. Volume expressed as cm^3/100 g unhydrated binder. CH: portlandite; Ht: hydrotalcite-like phase; Ms: calcium monosulfoaluminate.

- The rate of aluminate reaction in C_3S-gypsum-slag system was controlled by the availability of SO_4^{2-} and Al^{3+} ions, thus depending on the alumina content of slag and gypsum content added significantly.
- An approximatively linear correlation between SO_3 and Al_2O_3 contents in the system vs. heat release from aluminate reaction was found in most mixtures investigated. Also, the heat could be taken as an indication of the amount of ettringite formed.
- Calcium monosulfoaluminate occurred in C_3S-gypsum-slag A18 mixture from the first day, and its precipitation proceeded continuously with hydration at the expense of ettringite.
- Sulfur rich species incorporated in slag started to participate into the aluminate reaction after the main hydration peak of C_3S, and it played a similar role to gypsum. Therefore, it was suggested to take both alumina and sulfur content in slag into consideration when calculating SO_3/Al_2O_3 ratio.

CRediT authorship contribution statement

Yu Zhang: Investigation, Methodology, Experiment, Analysis, Writing – Original Draft preparation, Writing – Review & Editing.

Zhi Wan: Methodology, Experiment, Analysis, Review & Editing.

Luiz Miranda de Lima Junior: Experiment, Analysis, Review & Editing.

Oğuzhan Çopuroğlu: Supervision, Funding acquisition, Review & Editing.

Declaration of competing interest

The authors declare no conflict of interest.

Data availability

Data will be made available on request.

Acknowledgements

The authors are grateful for the China Scholarship Council (Grant Number 201808320456, 201906220205) and BAM Infraconsult B.V. for their financial support. Authors thank Arjan Thijssen (Microlab, TU Delft) for his technical support.

References

[1] L. Nicoleau, A. Nonat, D. Perrey, The di-and tricalcium silicate dissolutions, Cem. Concr. Res. 47 (2013) 14–30.
[2] L. Nicoleau, A. Nonat, A new view on the kinetics of tricalcium silicate hydration, Cem. Concr. Res. 86 (2016) 1–11.
[3] C. Naber, et al., Alite dissolution and CSH precipitation rates during hydration, Cem. Concr. Res. 115 (2019) 283–293.
[4] A. Quennoz, K.L. Scrivener, Hydration of C3A–gypsum systems, Cem. Concr. Res. 42 (7) (2012) 1032–1041.
[5] M.J. Sánchez-Herrero, A. Fernández-Jiménez, A. Palomo, Alkaline hydration of tricalcium aluminate, J. Am. Ceram. Soc. 95 (10) (2012) 3317–3324.
[6] A. Quennoz, K.L. Scrivener, Interactions between alite and C3A-gypsum hydrations in model cements, Cem. Concr. Res. 44 (2013) 46–54.
[7] S. Horkoss, R. Lteif, T. Rizk, Influence of the clinker SO3 on the cement characteristics, Cem. Concr. Res. 41 (8) (2011) 913–919.
[8] E.M.J. Berodier, EPFL, in: Impact of the Supplementary Cementitious Materials on the Kinetics and Microstructural Development of Cement Hydration, 2015.
[9] E. Özbay, et al., Utilization and efficiency of ground granulated blast furnace slag on concrete properties – a review, Constr. Build. Mater. 105 (2016) 423–434.
[10] N.E.A. De Belie, Properties of Fresh and Hardened Concrete Containing Supplementary Cementitious Materials Vol. 25, Springer, 2018.
[11] J. Skibsted, R. Snellings, Reactivity of supplementary cementitious materials (SCMs) in cement blends, Cem. Concr. Res. 124 (2019), 105799.
[12] J. Cheung, et al., Impact of admixtures on the hydration kinetics of Portland cement, Cem. Concr. Res. 41 (12) (2011) 1289–1309.
[13] M. Antoni, et al., Cement substitution by a combination of metakaolin and limestone, Cem. Concr. Res. 42 (12) (2012) 1579–1589.
[14] P.T. Durdziński, et al., Fly ash as an assemblage of model Ca–Mg–Na-aluminosilicate glasses, Cem. Concr. Res. 78 (2015) 263–272.
[15] F.A. Zunino Sommariva, EPFL, in: Limestone Calcined Clay Cements (LC3): Raw Material Processing, Sulfate Balance and Hydration Kinetics, 2020.
[16] FEhS, Hüttensand Datei, 2016.
[17] Y.-F. Chai, et al., Influencing mechanism of Al2O3 on sintered liquid phase of iron ore fines based on thermal and kinetic analysis, Ironmak. Steelmak. 46 (5) (2019) 424–430.
[18] Y. Xue, et al., Improving high-alumina iron ores processing via the investigation of the influence of alumina concentration and type on high-temperature characteristics, Minerals 10 (9) (2020) 802.
[19] F. Zunino, K. Scrivener, Factors influencing the sulfate balance in pure phase C3S/C3A systems, Cem. Concr. Res. 133 (2020).
[20] W.E. Kleinjan, et al., Kinetics of the chemical oxidation of polysulfide anions in aqueous solution, Water Res. 39 (17) (2005) 4093–4100.
[21] A. Gruskovnjak, et al., Hydration of alkali-activated slag: comparison with ordinary Portland cement, Adv. Cem. Res. 18 (3) (2006) 119–128.
[22] B. Lothenbach, et al., Hydration of a low-alkali CEM III/B–SiO2 cement (LAC), Cem. Concr. Res. 42 (2) (2012) 410–423.
[23] B. Bickmore, The effect of adsorbed Al(OH)4- on the dissolution rate of quartz, in: Eleventh Annual VM Goldschmidt Conference, 2001.
[24] X. Pardal, et al., 27Al and 29Si solid-state NMR characterization of calcium-aluminosilicate-hydrate, Inorg. Chem. Front. 51 (3) (2012) 1827–1836.
[25] T. Chappex, K.L. Scrivener, The effect of aluminum in solution on the dissolution of amorphous silica and its relation to cementitious systems, J. Am. Ceram. Soc. 96 (2) (2013) 592–597.
[26] L. Nicoleau, E. Schreiner, A. Nonat, Ion-specific effects influencing the dissolution of tricalcium silicate, Cem. Concr. Res. 59 (2014) 118–138.
[27] P. Suraneni, R.J. Flatt, Use of micro-reactors to obtain new insights into the factors influencing tricalcium silicate dissolution, Cem. Concr. Res. 78 (2015) 208–215.
[28] F. Begarin, et al., Hydration of alite containing aluminium, Adv. Appl. Ceram. 110 (3) (2011) 127–130.
[29] E. Pustovgar, et al., Influence of aluminates on the hydration kinetics of tricalcium silicate, Cem. Concr. Res. 100 (2017) 245–262.
[30] V. Kocaba, Development and Evaluation of Methods to Follow Microstructural Development of Cementitious Systems Including Slags, EPFL, 2009.
[31] S. Bergold, F. Goetz-Neunhoeffer, J. Neubauer, Interaction of silicate and aluminate reaction in a synthetic cement system: implications for the process of alite hydration, Cem. Concr. Res. 93 (2017) 32–44.
[32] I. Odler, J. Colán-Subauste, Investigations on cement expansion associated with ettringite formation, Cem. Concr. Res. 29 (5) (1999) 731–735.
[33] P. Chaunsali, P. Mondal, Hydration and early-age expansion of calcium sulfoaluminate cement-based binders: experiments and thermodynamic modeling, J. Sustain. Cement Based Mater. 5 (4) (2016) 259–267.
[34] F.P. Glasser, et al., Modification of cement pore fluid compositions by pozzolanic additives, Cem. Concr. Res. 18 (2) (1988) 165–178.
[35] A. Roy, Sulfur speciation in granulated blast furnace slag: an X-ray absorption spectroscopic investigation, Cem. Concr. Res. 39 (8) (2009) 659–663.
[36] K.Y. Chen, J.C. Morris, Kinetics of oxidation of aqueous sulfide by oxygen, Environ. Sci. Technol. 6 (6) (1972) 529–537.
[37] J. Couvidat, et al., Greening effect of concrete containing granulated blast-furnace slag composite cement: is there an environmental impact? Cem. Concr. Compos. 113 (2020), 103711.
[38] B. Mota, T. Matschei, K. Scrivener, The influence of sodium salts and gypsum on alite hydration, Cem. Concr. Res. 75 (2015) 53–65.
[39] H.F. Taylor, Cement Chemistry Vol. 2, Thomas Telford London, 1997.
[40] T. Wagner, et al., GEM-selektor geochemical modeling package: TSolMod library and data interface for multicomponent phase models, Can. Mineral. 50 (5) (2012) 1173–1195.
[41] D.A. Kulik, et al., GEM-selektor geochemical modeling package: revised algorithm and GEMS3K numerical kernel for coupled simulation codes, Comput. Geosci. 17 (1) (2013) 1–24.
[42] W. Hummel, Nagra Technical Report NTB 02-16. Wettingen, Switzerland, 2002.
[43] W. Hummel, et al., Nagra/PSI chemical thermodynamic data base 01/01, Radiochim. Acta 90 (9–11) (2002) 805–813.
[44] T. Matschei, et al., Thermodynamic properties of Portland cement hydrates in the system CaO–Al2O3–SiO2–CaSO4–CaCO3–H2O, Cem. Concr. Res. 37 (10) (2007) 1379–1410.
[45] B. Lothenbach, et al., Thermodynamic modelling of the effect of temperature on the hydration and porosity of Portland cement, Cem. Concr. Res. 38 (1) (2008) 1–18.
[46] R.J. Myers, S.A. Bernal, J.L. Provis, A thermodynamic model for C-(N-) ASH gel: CNASH_ss. Derivation and validation, Cem. Concr. Res. 66 (2014) 27–47.
[47] R.J. Myers, et al., Thermodynamic modelling of alkali-activated slag cements, Appl. Geochem. 61 (2015) 233–247.
[48] L. Mo, D.K. Panesar, Effects of accelerated carbonation on the microstructure of Portland cement pastes containing reactive MgO, Cem. Concr. Res. 42 (6) (2012) 769–777.
[49] M. Sajid, et al., Understanding the structure and structural effects on the properties of blast furnace slag (BFS), ISIJ Int. 59 (7) (2019) 1153–1166.
[50] V. Kocaba, E. Gallucci, K.L. Scrivener, Methods for determination of degree of reaction of slag in blended cement pastes, Cem. Concr. Res. 42 (3) (2012) 511–525.
[51] P. Termkhajornkit, et al., Dependence of compressive strength on phase assemblage in cement pastes: beyond gel–space ratio—experimental evidence and micromechanical modeling, Cem. Concr. Res. 56 (2014) 1–11.